Additive Manufacturing 36 (2020) 101522

Contents lists available at ScienceDirect

Additive Manufacturing

journal homepage: www.elsevier.com/locate/addma

Effects of Surface Energy Reducing Agents on Adhesion Force in Liquid Bridge Microstereolithography

Aslan Alamdari[a], Jeongwoo Lee[a], Myoeum Kim[a], Md. Omar Faruk Emon[a], Ali Dhinojwala[b], Jae-Won Choi[a,*]

[a] Department of Mechanical Engineering, The University of Akron, Akron, OH, 44325, USA
[b] Department of Polymer Science, The University of Akron, Akron, OH, 44325, USA

ARTICLE INFO

Keywords:
Vat photopolymerization
Microstereolithography
3D micro-printing
Liquid bridge
Surface energy reducing agent
Adhesion force

ABSTRACT

Projection microstereolithography (MSL) is a layer-by-layer manufacturing process used to fabricate three-dimensional (3D) microstructures. In this process, each layer of a photoreactive liquid resin is crosslinked by modulated ultraviolet (UV) light through a digital micromirror device (DMD). Despite the capabilities of MSL, there are some drawbacks such as incompatibility with highly viscous materials, long manufacturing time, large material consumption, and oxygen inhibition. To address these issues, liquid bridge microstereolithography (LBMSL) has been proposed as a vat-free process, which involves using a liquid resin supported by a capillary bridge between two substrates. One of the most important manufacturing steps in the LBMSL process is to detach the cured layers from the upper transparent substrate, without causing any damage to the structure during the 3D printing process. This paper has investigated the use of a small molecule additive, a surface energy reducing agent (SERA) that tends to migrate toward the transparent substrate and reduces adhesion at this interface. This has been proven through a series of adhesion force measurements and material characterization methods. The migration of SERA molecules has been studied using contact angle measurements and x-ray photoelectron spectroscopy (XPS). In addition, tensile measurements reveal that there are no detrimental effects on the mechanical properties of the resin due to adding SERA in the formulation. Multiple 3D microstructures have been fabricated to illustrate the advantage of adding SERA to reduce the adhesion of the resin to the transparent substrate in LBMSL.

1. Introduction

Additive manufacturing (AM) is a method of fabricating three dimensional parts in which materials are added using different methods to form structures from computer-aided design (CAD) models. Material extrusion, vat photopolymerization, powder bed fusion, and material jetting are popular AM processes used for different applications. These processes are selected based on desired requirements of mechanical properties, surface quality, accuracy, processing time, etc. [1]. Despite the recent advances in AM methods, there are still several technical challenges that need to be addressed. The focus of this paper is on using microstereolithography (MSL) as a method to manufacture objects with high resolution and surface quality [2–4] and enhancing its reliability. MSL is a photopolymerization process that polymerizes a liquid resin using UV light and it was first introduced by Ikuta et al. [5] and Takagi et al. [6] in 1993. Applications include microfluidics, ceramic parts, microelectromechanical system (MEMS) components, micro-optics, and structures for tissue engineering [7–14]. In addition, several mathematical modeling studies have been published to improve the quality and design of parts manufactured using MSL [15–24].

MSL methods using digital micromirror device (DMD) can be classified into two categories, bottom-up and top-down projection approaches, and both have their own advantages and deficiencies. In the top-down projection approach, layers are stacked on top of each other using modulated UV light reflecting through DMD. The major disadvantages of this technique are the inability to cure very thin layers of resin (due to the existence of oxygen in the air as a radical scavenger), long settling time for viscous resin, and possible curling of cured layers [10,16,25,26]. In comparison, the bottom-up projection technique, also known as the constrained surface technique, can address some of the limitations of the top-down approach. In this method, parts are manufactured using a transparent window as a bottom substrate in a vat of UV-curable resin. However, the disadvantage of this technique is the possibility that the cured layers adhere to the transparent window, as it

* Corresponding author.
E-mail address: jchoi1@uakron.edu (J.-W. Choi).

https://doi.org/10.1016/j.addma.2020.101522
Received 12 February 2020; Received in revised form 23 May 2020; Accepted 6 August 2020
Available online 10 August 2020

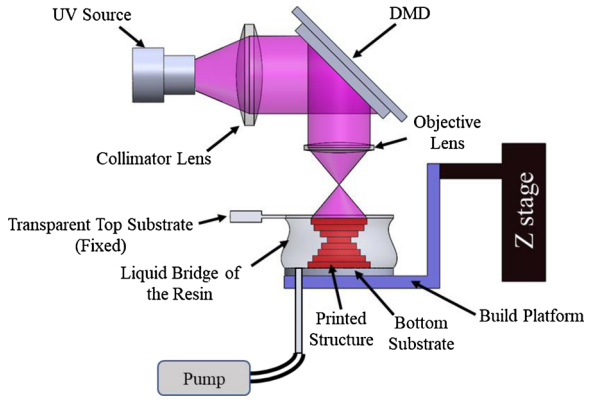

Fig. 1. Liquid Bridge Microstereolithography 3D Printing Method.

is difficult to detach this layer, and this may result in bad print quality [26,27].

Lee et al. [28,29] and Jo et al. [30] proposed a liquid bridge technique to enable the three-dimensional printing (3D printing) of structures without using a vat of resin. As illustrated in Fig. 1, parts are manufactured between two substrates with the resin held by a capillary bridge. The benefits of this approach include fast printing process, low material consumption, no oxygen inhibition due to the constraint of the material surface, and the option to use resins that are highly viscous. The important requirement is that the top substrate has to be transparent and should not adhere strongly to the cured layer (Fig. 2a) [28]. This problem cannot be simply solved by using low-energy surfaces because that would make it difficult to stabilize a liquid capillary bridge between the two substrates. Fig. 2b schematically illustrates the adhesion forces at both interfaces and the constraint in material selection for LBMSL. The main goal of the study is to overcome this limitation by reducing the adhesion of the cured resin to the top substrate, where the strong adhesion leads to the failure of the LBMSL process [31].

In some cases, the printing of a part by LBMSL will fail due to the partial detachment of the part from the upper transparent substrate. While overexposing the part to UV light would help to fix this issue, it would increase the adhesion force. LBMSL is limited to certain resins that will have lower surface energy at the interface with the transparent substrate than at the interface between the bottom substrate and the previously cured layers. The magnitude of the separation force is determined by the separation speed, exposure time, viscosity of the resin, temperature, and the geometry of the cured area [31,32].

Several technical and theoretical solutions have been proposed by researchers to address the adhesion force issue in the bottom-up projection stereolithography (SL) process. One of the best approaches is to coat the window with materials having a low surface energy (such as Teflon and silicone films); however, in most cases, the adhesion force would still be too high [26,33]. EnvisionTec uses a stretched Teflon coated glass for their commercial 3D printers. Zhou et al. [33] developed a peeling approach using a system where the window of the vat is divided into two channels, one of which is coated with polydimethylsiloxane (PDMS). As a new layer is cured, the platform moves horizontally to break the adhesion force that separates the part from the resin vat before it moves upward to provide fresh resin for the next layer. In another study, a vibration force provided by loudspeakers is used to reduce the separation force [34]; however, this vibration-assisted process only holds promise for the fabrication of parts with large cross sections, and it is not applicable for MSL.

Cohesive zone model (CZM) has been used to calculate the separation force [32] as a function of the detachment velocity. Liravi et al. [35] performed a finite element analysis that adopted CZM to create a closed-loop system that controls the separation speed to minimize the

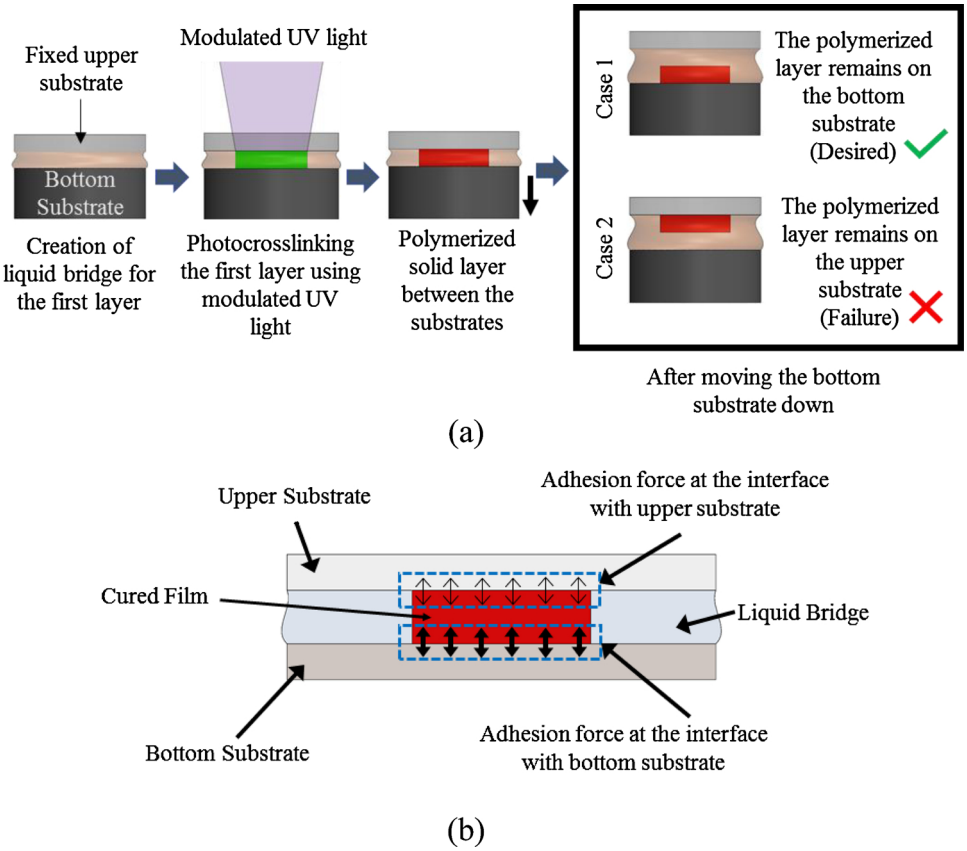

Fig. 2. Separation step in LBMSL: a) The two possible cases for a photopolymerized layer after the bottom substrate is pulled down; b) illustration of adhesion forces at the interfaces with the top and bottom substrate.

separation force. Even though optimizing the separation speed reduces the adhesion force, it is not sufficient to overcome this force. Tilting of the plates during separation has also been suggested to reduce the separation force. These forces were computed based on CZM methods, with an accompanying series of experimental data as verification [36].

Another proposed solution to achieve separation is the use of high concentrations of oxygen near the transparent window (by using oxygen permeating substrates), and this prevents a very thin layer of resin next to the window from undergoing polymerization. This thin layer of unpolymerized resin next to the transparent window reduces adhesion. Tumbleston et al. [37] developed continuous liquid interface production (CLIP) by taking the advantage of this phenomenon, which would prevent a very thin layer of resin (~20–30 μm in thickness and referred to as a dead zone) on the substrate from curing [38]. This technology has been implemented on Carbon M1 and M2 commercial 3D printers (Carbon3D Inc., Redwood City, CA, USA). However, this technique has not been investigated for the printing of microstructures with higher resolutions.

Palaganas et al. [39] have studied the effects of adding a liquid siloxane precursor in a commercial SL resin. One of the main benefits of adding a siloxane compound is the reduction in surface energy of resin, which has been verified using contact angle measurements in their study. However, this method has never been applied on any MSL techniques.

In this study, we demonstrate the addition of low-molecular-weight compounds (SERA), that tend to migrate toward the interface with glass substrate and reduce the adhesion force while maintaining the printing qualities. The SERA segments are not as strongly attached to the bottom poly(methyl methacrylate) (PMMA) substrate, which is useful in maintaining the necessary adhesion between the resin and the PMMA substrate. This asymmetric migration of SERA is important for LBMSL 3D printing.

2. Experimental Procedure

2.1. Materials

The photocrosslinkable resin used in this study consists of acrylate-based commercial monomers, a photoinitiator, a light absorber to control the cure depth, and SERA to reduce the adhesion force. The base resin was prepared by mixing photocurable monomers such as isobornyl acrylate (IBXA), 1,6-hexanediol diacrylate (HDDA), and bisphenol-A-ethoxylate (4) diacrylate (BEDA), blended in ratios of 4.5:4.5:1 by wt.%. 1 wt.% of 2,2-dimethoxy-2-phenylacetophenone (DMPA) was added as a photoinitiator. The monomers and the photoinitiator were purchased from Sigma-Aldrich (St. Louis, MO, USA). To this mixture, 0.15 wt.% of Tinuvin 327™ (Ciba, Timonium, MD, USA) was added as the light absorber because of its high absorption (~40 percent) at 365 nm [19]. The materials were mixed for 20 minutes at room temperature using a mixer (SpeedMixer, FlackTek Inc., Landrum, SC, USA).

Different concentrations of BYK-UV 3500 (BYK Additives & Instruments, Louisville, KY) as SERA, a curable acryl-functional polydimethylsiloxane, were dissolved in the base resin to study the effect of SERA on the separation force. The silicon segments of the SERA (shown in the schematic diagram of the chemical structure of SERA in Fig. 3) play an important role in the distribution of the SERA in the resin. The silicon segments typically tend to migrate toward the surface of the resin, enhancing its hydrophobicity. However, as the SERA concentration in the resin is increased, the cohesive interactions between the segments become more significant, and the segments begin to form groups inside the resin through accumulation, reducing the area available to interface with the polar substrate used to form a liquid bridge [40]. A minimum of 10 experiments were performed for each of the concentrations to measure the separation force. The substrates used in this study were circular-shaped plates (12 mm in diameter) made using two different materials: glass and PMMA. The glass plate was used as the top substrate, and the PMMA plate was used as the bottom substrate.

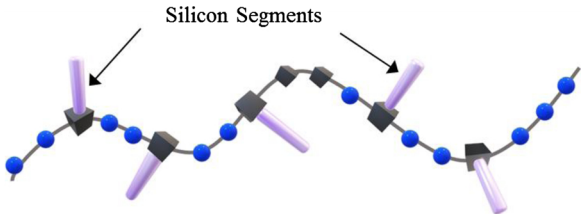

Fig. 3. Schematic of the chemical structure of the surface energy reducing agent.

2.2. Overview of the liquid bridge microstereolithography system

The LBMSL technique is a layer-by-layer top-down projection process that uses different subsystems to manipulate and modulate UV light with proper exposure and layer thickness control. The main components of this system include a UV source (an OmniCure S2000 mercury lamp filtered at a wavelength of 365 nm, obtained from Excelitas Technologies Co.), a light modulating system (a series of lenses, a mirror, DMD and a controller obtained from Texas Instruments), and a moving platform (an Aerotech Z-stage with a resolution of 500 nm, obtained from Aerotech Inc., Pittsburgh, PA, USA) [18,28]. In the setup used for this study, the top transparent substrate was fixed, and the bottom disk was installed on the Z-stage. A liquid bridge was created between the two circular substrates, which were fixed in a parallel coaxial configuration. The resin was supplied by an NE-1000 syringe pump (from New Era Pump Systems Inc., Farmingdale, NY, USA) with a minimum pumping rate of 0.73 μl/hr. Using this LBMSL setup, parts with a layer thickness as thin as 1 μm can be built due to the absence of oxygen in the liquid bridge, which prohibits oxygen inhibition from occurring [18,28]. More details about the LBMSL method can be found in the prior work [28].

2.3. Characterizations

2.3.1. Adhesion force

The experimental setup for the adhesion test is illustrated in Fig. 4. A Mark-10 Series 5 force gauge (M5-5, Mark-10 Corp., Copiague, NY, USA) was used to measure the separation force with a sampling rate of 250 Hz, and it was integrated with a MATLAB program to capture the data. A circular 2D pattern with a diameter of 1.8 mm was projected on the liquid bridge to cure the resin using a light irradiance of ~9.6 mW/cm^2 and an exposure time of 6 seconds. After a 10-μm thin film was polymerized, the Z platform was moved downward at a speed of 0.5 mm/s in order to detach the film from the top substrate. The amount of resin used to create the liquid bridge was 30 μl. Before starting each experiment, the substrates were cleaned using ethanol and were dried by gentle air blowing to prevent contamination and minimize errors. Care was taken to ensure that the syringe was free of

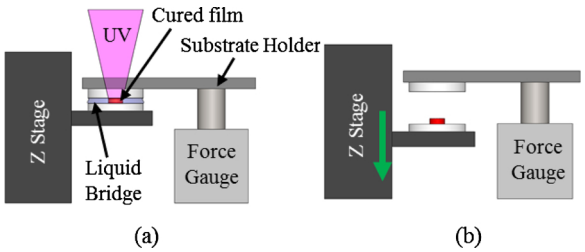

Fig. 4. Experimental setup for detachment tests. a) a cured film between the substrates in the liquid bridge before separation and b) after separation.

bubbles, since bubbles contain oxygen and would cause defects in the liquid bridge, which would affect the adhesion force. At least 10 experiments were performed for each concentration of SERA to measure the separation force.

2.3.2. Contact angle

A Ramé-Hart contact angle goniometer (Ramé-Hart Instrument Co., Succasunna, NJ, USA) was used to determine the contact angles for 5-μl droplets of resins having different concentrations of SERA on a glass substrate. The contact angles for each material were measured using *ImageJ* image processing software (a Java-based program developed at the National Institutes of Health and the Laboratory for Optical and Computational Instrumentation at the University of Wisconsin).

2.3.3. SERA distribution

X-ray photoelectron spectroscopy using an XPS PHI 5000 Versa Probe II (from Physical Electronics, Inc., Chanhassen, MN, USA) was employed to investigate the migration of SERA segments toward the glass substrate in the cured films for resins with different weight percentages of SERA. Spot sizes of 50 μm were used to study six equally spaced points on each sample.

The samples used for studying the SERA distribution in the liquid bridge were prepared as illustrated in Fig. 5. The samples have a thickness of 1.2 mm, which is large enough to enable the distribution of silicon segments in the sample cross section to be clearly observed. All resin formulations in between the two substrates were fully polymerized by a flood of UV light; after polymerization, the samples were broken manually from their centers, and the cross sections were studied using XPS analysis. The samples were not washed using any solvents, and the cross sections were free from exposure to any chemicals. The frame (shown in Fig. 4a) that was used to produce the samples was 3D printed using a commercial 3D printer (Replicator+, MakerBot Industries, Brooklyn, NY, USA).

To qualitatively investigate the manufacturability of the materials using LBMSL, the 3D printed structures were observed using an FEI Quanta 200 environmental scanning electron microscope (ESEM, FEI Company, Hillsboro, OR, USA).

2.3.4. Mechanical properties

To investigate the effect of SERA on the mechanical properties of the polymerized parts, tensile tests were performed using an Instron 5582 universal testing machine (Instron, Norwood, MA, USA) with a 500-N load cell transducer at room temperature (24 ± 1 °C) to obtain the Young's modulus and strength of materials with different concentrations of SERA. Type IV tensile specimens from ASTM D638-14 were used (Fig. 6). The fabricated specimens were tested at a constant strain rate of 5 mm/min. Seven sets of materials (with 0, 1, 3, 5, 10, 15, and 20 wt.% of SERA) were included in the tests. The dimensions of each tensile bar (overall length, overall width, and thickness) were measured using digital calipers with a precision of 0.01 mm. At least six tensile bars were tested for each material.

Due to the limitation in the size of the working area of the current LBMSL setup, it was not possible to 3D print tensile bars with the original dimensions specified in ASTM D638-14. An alternative method is

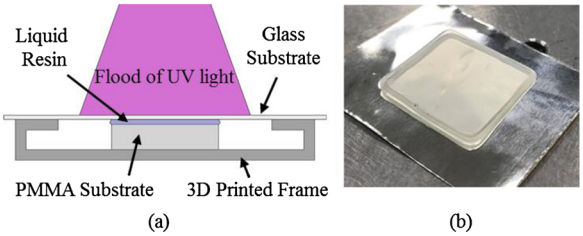

Fig. 5. XPS samples preparation a) the setup of creating a 1.2 mm thick layer, b) a photo of polymerized sample.

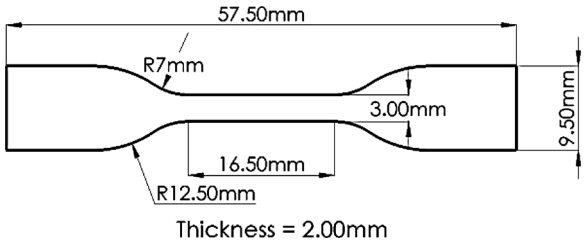

Fig. 6. Dimensions of tensile test specimen (ASTM D638-14).

to fabricate specimens using molds. The tensile bars were 50% scaled down since SERA affects the critical exposure E_c and penetration depth D_p of the resin at higher concentrations (above 10 wt.%), which makes it impossible to fabricate specimens in the original size. The downscaled samples were manufactured using a silicone mold fabricated by a commercial 3D printer - Form2 (Formlabs, Somerville, MA, USA). In the process shown in Fig. 7, an Ecoflex 00-30 silicone mold material was used to create a mold of 3D printed specimen. A liquid resin was then poured into the mold and transparent sheets of polyethylene terephthalate (PET) were used to cover the mold to avoid oxygen inhibition and allow the resin to completely polymerize. The samples (which were free from bubbles, defects, and impurities), were then exposed to a flood of UV light using an OmniCure S200 (Excelitas Technologies Co., Waltham, MA, USA) until they were fully polymerized. Once the samples were fully cured, they were removed from the silicone mold.

3. Results and Discussion

3.1. Adhesion force and contact angle measurements

After exposing each constrained layer to modulated UV light in the LBMSL setup to polymerize a circular disk, adhesion forces on the interfaces with the top and bottom substrates are generated. Since LBMSL is a top-down procedure, the adhesion force between the printed layer and the bottom substrate must be stronger than that between the printed layer and the upper substrate in order to hold the part during the print. In this research, a base resin (resin without SERA) was intentionally chosen that creates a stronger adhesive bond with the glass substrate, making the base resin incompatible for use with LBMSL. After the addition of SERA, however, the adhesion force decreased, and the resin was able to create a stronger bond with the PMMA substrate than with the glass, resulting in the printed layers being held on the bottom substrate. Consequently, the addition of SERA to the base resin allowed the structures to be printed successfully.

A series of detachment experiments were performed to measure the separation force between the cured layer and the glass substrate. Since it is known that the separation force is dependent on the detachment velocity and layer thickness [26,32], these parameters were kept constant throughout the tests. Fig. 8 reveals that the separation force decreases as the amount of SERA is increased in the resin, and this result was expected. The concentration gradient of the SERA segments inside the liquid bridge leads to this variation in adhesion force [39,41,42].

Another method to investigate the reduction in adhesion force is to measure the contact angles of droplets with different SERA concentrations on a glass substrate, since surface energy is known to be proportional to the contact angle and/or the interfacial area. As illustrated in Fig. 9, for low SERA concentrations, the contact angle increased due to the tendency of the SERA segments to migrate toward the surface, and especially toward the glass interface because of their polarity attraction. In this situation, the segments tend to accumulate at the interface, resulting in a reduction in the adhesion force and an increase in the contact angle[39]. However, at higher concentrations of SERA, due to the cohesive interactions between SERA segments, the behavior of the segments changes, and they begin to accumulate and form groups

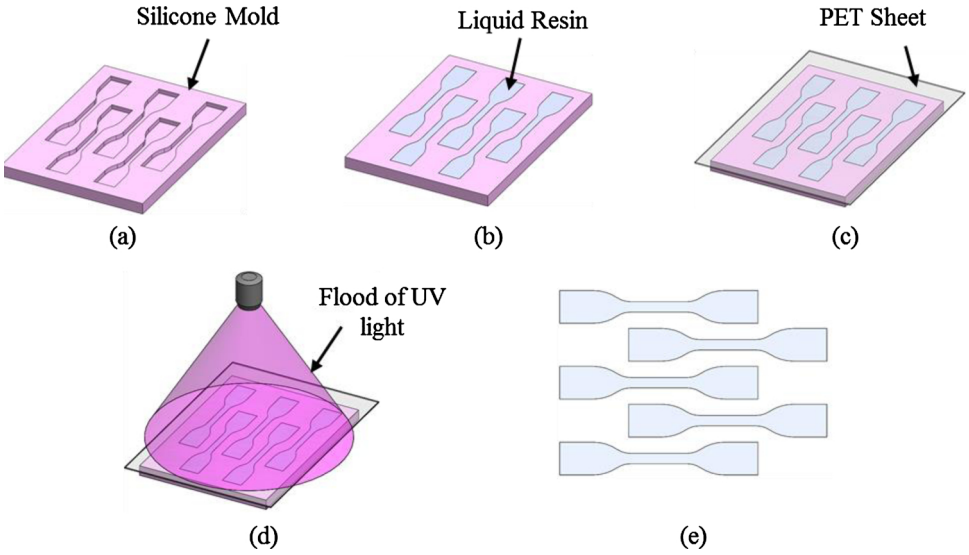

Fig. 7. Tensile bar fabrication: a) mold b) liquid resin added c) transparent PET sheet on top of the mold d) UV light exposure e) fabricated parts.

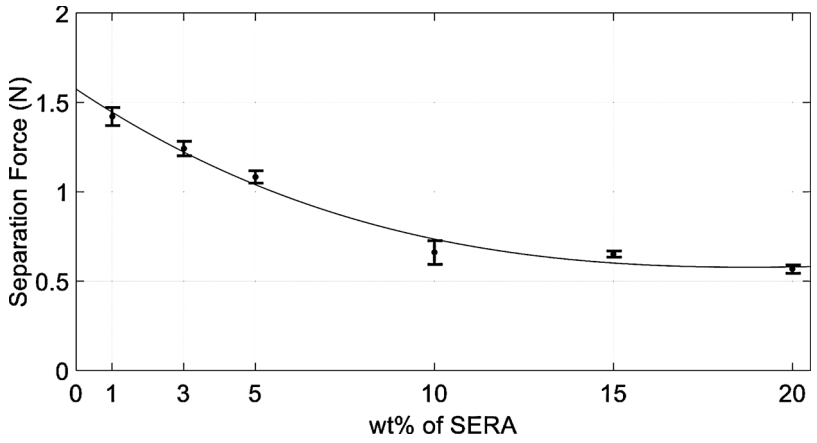

Fig. 8. Separation force for samples having different concentrations of SERA.

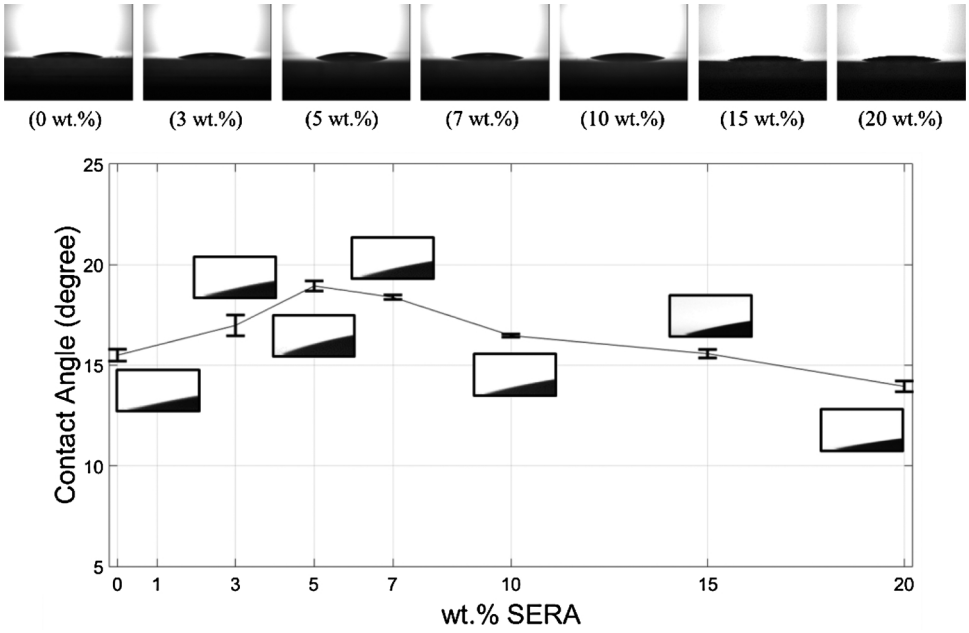

Fig. 9. Contact angles of the resin droplets on a glass substrate.

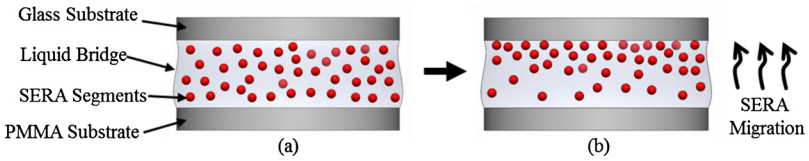

Fig. 10. SERA migration: a) Initial distribution of SERA segments, and b) migration of SERA segments toward the glass substrate.

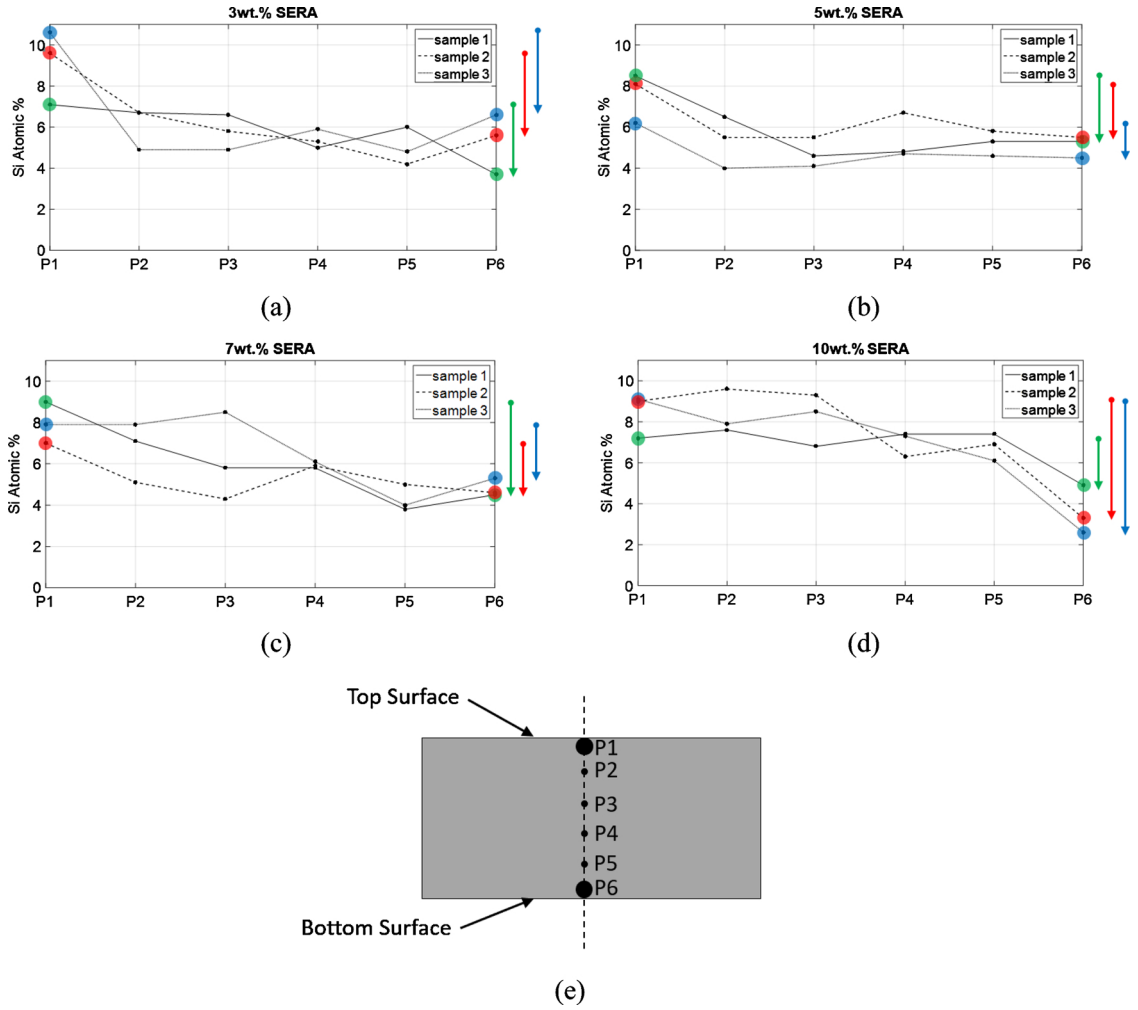

Fig. 11. XPS results for cured samples with a) 3 wt.%, b) 5 wt.%, c) 7 wt.%, and d) 10 wt.% of SERA, where the vertical arrows indicate the amount of the Si atom% variation from P1 to P6 for each sample, e) schematic cross section of an XPS sample.

inside the droplets; as a result, their interface with glass is reduced. In fact, the presence of SERA segments on the surface and/or interface reduces the adhesion, not their presence inside the resin. This explains why the contact angles are reduced for resins having SERA concentrations higher than 5 wt.% [40].

Since the conditions in the two sets of adhesion evaluations are not the same, exact correlations between them cannot be easily made. For example, it cannot necessarily be concluded that the resin must have the lowest separation force at 5 wt.% based on the contact measurements. In the liquid bridge, the distribution of SERA segments is somewhat different than that in a droplet on glass. Since the resin is trapped between two circular substrates and glass has a stronger polarity attraction than PMMA, most (but not all) of the SERA segments will move toward the glass. In addition, since the layer thickness is 10 μm and the diameter of the plates is 12 mm, the segments in the liquid bridge cannot easily begin to form large groups (as compared to the segments in the resin droplets), and the segments mostly appear at the interfaces. However, in the contact angle measurements obtained in this study, the resin was only interacting with glass, and the size and volume of the droplets (5 μl droplets with a diameters of ~ 3.7 mm and a height of ~ 200 μm) provide more room for SERA groups inside the resin. Therefore, it is concluded that SERA reduces the adhesion force to some extent, depending on its distribution in the resin. This will be further explained in the discussion section.

3.2. X-ray photoelectron spectroscopy (XPS)

This section describes the results of X-ray photoelectron spectroscopy (XPS) tests that were conducted to study the distribution of the SERA segments. When a liquid bridge is formed between the substrates, the SERA segments will tend to move toward the glass based on their polarity [40], which reduces the separation force between each cured film and glass as mentioned in the previous section. A schematic illustration of this phenomenon is provided in Fig. 10.

Since SERA contains silicon (Si), XPS elemental analyses can be utilized to study the distribution of Si between the top and bottom edges of each 1.2-mm-thick cured sample to prove our hypothesis. As shown on Fig. 11e, six equally spaced points across the cross section of

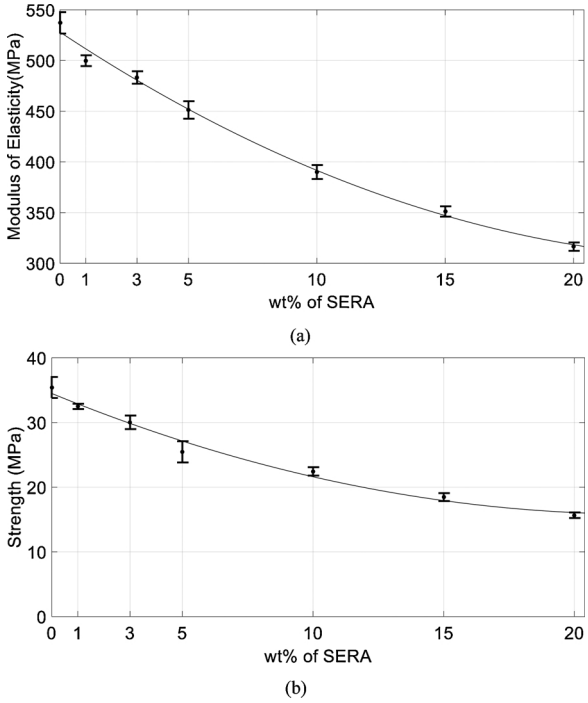

Fig. 12. Mechanical properties for different concentrations of SERA.

each sample were investigated for this study. Point P1 is a point in the vicinity of the top edge, where the liquid bridge was in contact with glass, and Point P6 is located at the bottom edge, at a place where the liquid bridge is in contact with PMMA. The XPS results for materials having 3, 5, 7, and 10 wt.% SERA are provided in Fig. 11, in which the values obtained for each replicate are reported. The data reveal the migration of SERA segments toward the glass substrate, since in all samples, the atomic percent of Si at Point P1 is higher than that at Point P6. This significant difference has also been verified using t-test between these two points. As discussed before, the samples were intentionally fabricated to have a greater thickness than those used for LBMSL in order to study the Si distribution along the thickness of the samples. However, this larger volume of resin allows the segments to form groups with different sizes due to their tendency to accumulate while they were being attracted to the glass. Therefore, since the distribution would not be symmetric and homogeneous across each sample, the values for each sample are reported separately (rather than reporting only an average value for the three measurements obtained at the same location). According to Fig. 11, at 3 wt.%, 5 wt.%, and 7 wt.%, the SERA segments tend to move toward the upper substrate; however,

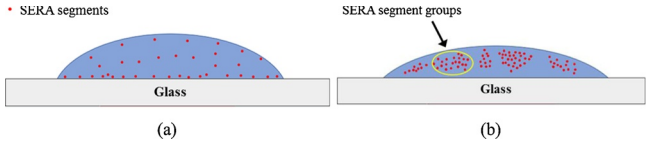

Fig. 14. Schematic of SERA distribution in droplets for a) lower concentrations and b) higher concentrations of SERA.

at 10 wt.%, the cohesive interaction between segments becomes stronger, since higher percentages of Si can be observed in the intermediate points (P2 to P5). This trend indicates that larger SERA groups were formed inside the resin than at the top or bottom edges.

3.3. Tensile tests

To determine the elastic modulus, *E*, and the ultimate tensile strength of the specimens, a series of tensile tests were performed. The elastic moduli were calculated as the slope of the initial linear portion of the stress–strain curve through linear fitting of the data. The tensile strength was defined as the stress at failure carried by the specimen during the tensile test. Fig. 12 reveals that as more SERA is added to the material, the modulus of elasticity decreases and strength for the polymerized material becomes lower. This expected result is consistent with the result from the prior work [39] on adding a siloxane compound to a commercial resin.

Based on statistical analysis on the tensile data, SERA starts to significantly affect both of the mechanical properties at 3 wt.% concentration. Additionally, there is no significant difference between the properties of 15 wt.% and 20 wt.% concentrations which implies that only a certain amount of SERA can participate in the crosslinking and the rest remains unpolymerized. A simple experiment was conducted to investigate effects of SERA on the degree of polymerization. For this purpose, samples of each polymerized group of materials were soaked in ethanol for 24 hours to remove the residual resin (the unpolymerized resin) and then the samples were dried in an oven at 80 °C for 12 hours. Original samples (before the experiment) and dried samples (after the experiment) were weighed and compared. The results indicate that the degree of polymerization decreases from 95.37% for the resin with no SERA to 77.95% for the resin with 20 wt.% of SERA. In general, the introduction of this additive reduces the mechanical properties of the material; however, at 5 wt.%, the material shows promising results in terms of manufacturing with high resolution, as discussed in the following section.

3.4. Manufactured Parts

One of the important issues related to incorporating a surface

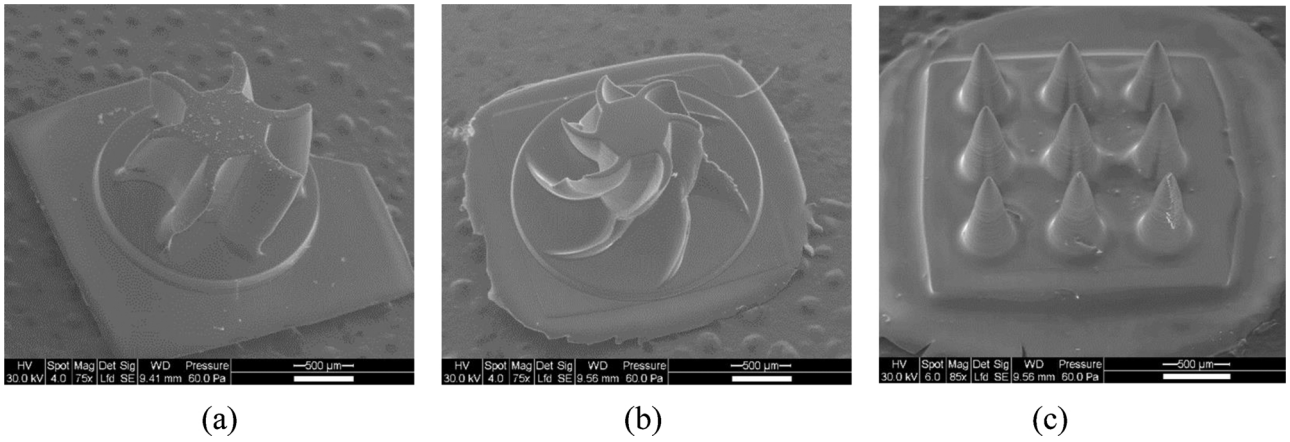

Fig. 13. SEM images of manufactured microstructures with 5 wt.% of added SERA (scale bar: 500 μm): (a) a fan 1, (b) fan 2, and (c) an array of microneedles.

energy reducing agent into the resin is to prove the manufacturability of the SERA-loaded material. Since the base resin has a light absorber, the penetration depth can be controlled and a proper set of printing parameters can be identified [19]. In this study, several 3D microstructures were fabricated to assess the manufacturability of the resin after adding SERA. These parts were manufactured using an irradiance of ~9.6 mW/cm^2 and a layer thickness of 5 μm. An exposure time of 6 seconds was used for the part shown in Fig. 13a and an exposure time of 9 seconds was used for the parts shown in Fig. 13b and c. The printing parameters depend on the material and geometry of each part, and these parameters were determined empirically. However, for some structures that are composed of large and small features, it is not possible to find a good set of exposure parameters due to light scattering. In these situations, a compromise between obtaining different features of the structure is required. For instance, part b has tapered blades with not fully polymerized edges. For this part, if each layer gets longer UV exposure, the sharpness of the internal edges, where the blades are connected to the middle shaft, would be lost while the outer edges of each blade would receive enough exposure to get polymerized. This contradicting effects are under investigations with multiple exposure.

The best parts were manufactured using 5 wt.% SERA, in which the adhesion force is sufficiently low, and high resolutions can be achieved in printing. For higher weight percentages of SERA, the manufacturability may be reduced in terms of resolution, while for lower concentrations, the higher adhesion force can damage the surface quality of the structures and can sometimes result in failure during the printing. The part shown in Fig. 13c features an array of microneedles having a 400-μm-diameter base and a height of 1000 μm.

3.5. Discussion

The goal of adding SERA into the resin is to reduce the adhesion force at the interface of the most recent polymerized layer and the top glass substrate. The results of the detachment experiments presented in Section 3.1 indicate a high probability that this additive can be used for the LBMSL process. In addition, the contact angle measurements show a reduction in surface energy for low concentrations of SERA; however, for higher concentrations, it has the negative effect. This can be addressed by understanding the behavior of the SERA segments. According to a previous report [41], SERA molecules tend to migrate toward the surface and interfacial areas of the resin; however, when the amount of SERA is increased, the cohesive interactions between the SERA segments cause them to accumulate and form groups in random sizes. This causes some randomness in their distribution inside the resin. The gravity, size of the formed groups, density differences between the phase separated groups and the rest of the resin, the existence of glass as a polar material, etc. may play certain roles in the distribution of segments. This can explain the inconsistency in the XPS analysis results presented in Fig. 11. However, there are consistent results indicating that a larger amount of SERA is distributed in the vicinity of the glass substrate than in the bottom PMMA substrate for all samples. This explains why there is a significant reduction in the adhesion force at this interface. For the contact angle measurements, the schematic distribution of segments is illustrated in Fig. 14 for low and high concentrations of SERA. In addition, the contact angles shown in Fig. 9 were measured when the droplets had settled on the glass substrate. It was observed that there is a difference between the initial and settled angle of the droplets for different concentrations of SERA. All droplets were also measured as they were placed on the substrate and after they had settled (after ~10 seconds). The average differences between the initial and settlement angles were 0.04, 0.50, 0.90, 1.18, 1.78, 2.94, and 3.33 degrees for 0, 3, 5, 7, 10, 15, and 20 weight percentages of SERA, respectively. This observation supports the hypothesis that the distribution of SERA segments is a function of time and that these segments are forming groups inside the droplets (not at the interface or the surface), which explains the inconsistency noted in the XPS results for the middle points (P2 to P5) of the sample.

4. Conclusion

In summary, this study investigated the effects of a surface energy reducing agent (SERA) on the reduction of the adhesion force in liquid bridge microstereolithography. By introducing this additive, a resin that was not printable using LBMSL would become compatible for the manufacture of 3D microstructures. The migration of silicon segments of the SERA toward the transparent glass substrate was confirmed by XPS elemental analysis. The contact angle measurements support the adhesion and XPS test results. This study also shows that for a specific resin, a proper amount of SERA can be added to reduce the adhesion force. Mechanical testing of fabricated tensile bars showed that a material with an elastic moduli in the range of 320 MPa to 540 MPa is suitable for use in various applications. The 3D printed microstructures demonstrated good printing accuracy and the feasibility of this approach. Applying this method would enable a larger group of materials to be compatible for LBMSL 3D printing with the desired specifications by tuning the material formulae and adding a SERA.

Statement on Conflicts of Interest

One of the authors of this article is part of the editorial board of the journal. To avoid potential conflicts of interest, the responsibility for the editorial and peer-review process of this article lies with the other editors of the journal. Furthermore, the authors of this article were removed from the peer review process and have no access to confidential information related to the editorial process of this article.

Declaration of Competing Interest

The authors declare that they have no known competing financial interests or personal relationships that could have appeared to influence the work reported in this paper.

CRediT authorship contribution statement

Aslan Alamdari: Investigation, Methodology, Data curation, Writing - Original draft preparation, Writing - review & editing.

Jeongwee Lee: Conceptualization, Methodology. Formal analysis.

Myoeum Kim: Methodology, Data curation.

Md. Omar Faruk Emon: Methodology, Data curation.

Ali Dhinojwala: Conceptualization, Methodology.

Jae-Won Choi: Conceptualization, Methodology, Funding acquisition, Supervision, Writing - review & editing.

Acknowledgements

This work was supported by the National Science Foundation under grant no. CMMI MME-1636118.

References

[1] I. Gibson, D.W. Rosen, B. Stucker, Introduction and Basic Principles, Additive Manufacturing Technologies: Rapid Prototyping to Direct Digital Manufacturing, Springer US, Boston, MA, 2010, pp. 20–35.
[2] I. Gibson, D.W. Rosen, B. Stucker, Photopolymerization Processes, Additive Manufacturing Technologies: Rapid Prototyping to Direct Digital Manufacturing, Springer US, Boston, MA, 2010, pp. 78–119.
[3] J.W. Choi, Y.M. Ha, K.H. Choi, S.H. Lee, Fabrication of 3-dimensional microstructures using dynamic image projection, Progress of Precision Engineering and Nano Technology 339 (2007) 473.
[4] S.C. Ligon, R. Liska, J. Stampfl, M. Gurr, R. Mulhaupt, Polymers for 3D Printing and Customized Additive Manufacturing, Chemical Reviews 117 (15) (2017) 10212–10290.
[5] K. Ikuta, K. Hirowatari, Real three dimensional micro fabrication using stereo lithography and metal molding, (1993).
[6] T. Takagi, N. Nakajima, Photoforming applied to fine machining, (1993).

[7] J.W. Choi, R. Wicker, S.H. Lee, K.H. Choi, C.S. Ha, I. Chung, Fabrication of 3D biocompatible/biodegradable micro-scaffolds using dynamic mask projection microstereolithography, Journal of Materials Processing Technology 209 (15-16) (2009) 5494–5503.
[8] K.J. Zhong, Y.Q. Gao, F. Li, N.N. Luo, W.W. Zhang, Fabrication of continuous relief micro-optic elements using real-time maskless lithography technique based on DMD, Optics and Laser Technology 56 (2014) 367–371.
[9] R. Gauvin, Y.C. Chen, J.W. Lee, P. Soman, P. Zorlutuna, J.W. Nichol, H. Bae, S.C. Chen, A. Khademhosseini, Microfabrication of complex porous tissue engineering scaffolds using 3D projection stereolithography, Biomaterials 33 (15) (2012) 3824–3834.
[10] X. Song, Y. Chen, T.W. Lee, S.H. Wu, L.X. Cheng, Ceramic fabrication using Mask-Image-Projection-based Stereolithography integrated with tape-casting, Journal of Manufacturing Processes 20 (2015) 456–464.
[11] A. Bertsch, P. Renaud, C. Vogt, P. Bernhard, Rapid prototyping of small size objects, Rapid Prototyping Journal 6 (4) (2000) 259–266.
[12] J.W. Lee, P.X. Lan, B. Kim, G. Lim, D.W. Cho, 3D scaffold fabrication with PPF/DEF using micro-stereolithography, Microelectronic Engineering 84 (5-8) (2007) 1702–1705.
[13] Y.F. Lu, S.N. Mantha, D.C. Crowder, S. Chinchilla, K.N. Shah, Y.H. Yun, R.B. Wicker, J.W. Choi, Microstereolithography and characterization of poly(propylene fumarate)-based drug-loaded microneedle arrays, Biofabrication 7 (4) (2015).
[14] N.A. Chartrain, C.B. Williams, A.R. Whittington, A review on fabricating tissue scaffolds using vat photopolymerization, Acta Biomaterialia 74 (2018) 90–111.
[15] C. Sun, N. Fang, D.M. Wu, X. Zhang, Projection micro-stereolithography using digital micro-mirror dynamic mask, Sensors and Actuators a-Physical 121 (1) (2005) 113–120.
[16] A.S. Jariwala, F. Ding, A. Boddapati, V. Breedveld, M.A. Grover, C.L. Henderson, D.W. Rosen, Modeling effects of oxygen inhibition in mask-based stereolithography, Rapid Prototyping Journal 17 (3) (2011) 168–175.
[17] A.S. Limaye, D.W. Rosen, Process planning method for mask projection micro-stereolithography, Rapid Prototyping Journal 13 (2) (2007) 76–84.
[18] J.W. Choi, Y.M. Ha, S.H. Lee, K.H. Choi, Design of microstereolithography system based on dynamic image projection for fabrication of three-dimensional microstructures, Journal of Mechanical Science and Technology 20 (12) (2006) 2094–2104.
[19] J.W. Choi, R.B. Wicker, S.H. Cho, C.S. Ha, S.H. Lee, Cure depth control for complex 3D microstructure fabrication in dynamic mask projection microstereolithography, Rapid Prototyping Journal 15 (1) (2009) 59–70.
[20] C. Zhou, Y. Chen, R.A. Waltz, Optimized Mask Image Projection for Solid Freeform Fabrication, Journal of Manufacturing Science and Engineering-Transactions of the Asme 131 (6) (2009).
[21] C. Zhou, Y. Chen, Calibrating Large-area Mask Projection Stereolithography for Its Accuracy and Resolution Improvements, (2009).
[22] H.W. Kang, J.H. Park, D.W. Cho, A pixel based solidification model for projection based stereolithography technology, Sensors and Actuators a-Physical 178 (2012) 223–229.
[23] M.M. Emami, F. Barazandeh, F. Yaghmaie, An analytical model for scanning-projection based stereolithography, Journal of Materials Processing Technology 219 (2015) 17–27.
[24] F.P.W. Melchels, J. Feijen, D.W. Grijpma, A review on stereolithography and its applications in biomedical engineering, Biomaterials 31 (24) (2010) 6121–6130.
[25] K. Xu, Y. Chen, Asme, Curing temperature study for curl distortion control and simulation in projection based Stereolithography, Proceedings of the Asme International Design Engineering Technical Conferences and Computers and Information in Engineering Conference 1a (2014) (2014).
[26] Y.-M. Huang, C.-P. Jiang, On-line force monitoring of platform ascending rapid prototyping system, Journal of Materials Processing Technology 159 (2) (2005) 257–264.
[27] P.M. Lambert, E.A. Campaigne Iii, C.B. Williams, Design considerations for mask projection microstereolithography systems, (2013).
[28] J. Lee, Y. Lu, S. Kashyap, A. Alarmdari, M.O.F. Emon, J.-W. Choi, Liquid bridge microstereolithography, Additive Manufacturing 21 (2018) 76–83.
[29] Y.F. Lu, J. Lee, S. Kashyap, M.O.F. Emon, J.W. Choi, Asme, Development and characterizations of Liquid Bridge Based Microstereolithography (LBMSL) system, Proceedings of the Asme 12th International Manufacturing Science and Engineering Conference 2 (2017) (2017).
[30] K.H. Jo, S.H. Lee, J.W. Choi, Liquid Bridge Stereolithography: A Proof of Concept, International Journal of Precision Engineering and Manufacturing 19 (8) (2018) 1253–1259.
[31] C. Decker, Kinetic study and new applications of UV radiation curing, Macromolecular Rapid Communications 23 (18) (2002) 1067–1093.
[32] H. Ye, A. Venketeswaran, S. Das, C. Zhou, Investigation of separation force for constrained-surface stereolithography process from mechanics perspective, Rapid Prototyping Journal 23 (4) (2017) 696–710.
[33] C. Zhou, Y. Chen, Z.G. Yang, B. Khoshnevis, Digital material fabrication using mask-image-projection-based stereolithography, Rapid Prototyping Journal 19 (3) (2013) 153–165.
[34] J. Jin, J.F. Yang, H.C. Mao, Y. Chen, A vibration-assisted method to reduce separation force for stereolithography, Journal of Manufacturing Processes 34 (2018) 793–801.
[35] F. Liravi, S. Das, C. Zhou, Separation force analysis and prediction based on cohesive element model for constrained-surface Stereolithography processes, (2015).
[36] X.Q. Wu, Q. Lian, D.C. Li, Z.M. Jin, Tilting separation analysis of bottom-up mask projection stereolithography based on cohesive zone model, Journal of Materials Processing Technology 243 (2017) 184–196.
[37] J.R. Tumbleston, D. Shirvanyants, N. Ermoshkin, R. Janusziewicz, A.R. Johnson, D. Kelly, K. Chen, R. Pinschmidt, J.P. Rolland, A. Ermoshkin, E.T. Samulski, J.M. DeSimone, Continuous liquid interface production of 3D objects, Science 347 (6228) (2015) 1349–1352.
[38] A.R. Johnson, C.L. Caudill, J.R. Tumbleston, C.J. Bloomquist, K.A. Moga, A. Ermoshkin, D. Shirvanyants, S.J. Mecham, J.C. Luft, J.M. DeSimone, Single-Step Fabrication of Computationally Designed Microneedles by Continuous Liquid Interface Production, Plos One 11 (9) (2016).
[39] J. Palaganas, A.C. de Leon, J. Mangadlao, N. Palaganas, A. Mael, Y.J. Lee, H.Y. Lai, R. Advincula, Facile preparation of photocurable siloxane composite for 3D printing, Macromolecular Materials and Engineering 302 (5) (2017) 1600477.
[40] M. Esmaeilpour, B. Niroumand, A. Monshi, B. Ramezanzadeh, E. Salahi, The role of surface energy reducing agent in the formation of self-induced nanoscale surface features and wetting behavior of polyurethane coatings, Progress in Organic Coatings 90 (2016) 317–323.
[41] N. Naseh, M. Mohseni, B. Ramezanzadeh, Role of surface active additives on reduction of surface free energy and enhancing the mechanical Attributes of easy-to-clean automotive clearcoats: Investigating resistance against simulated tree gum, International Journal of Adhesion and Adhesives 44 (2013) 209–219.
[42] M. Esmaeilpour, B. Niroumand, A. Monshi, E. Salahi, B. Ramezanzadeh, Effects of Curing Condition on the Surface Characteristics of Two-pack Polyurethane Coatings Containing Low Surface Energy Additive, Soft Materials 13 (3) (2015) 144–149.